

## Uni-axial behavior of energy dissipative steel cushions

Hasan Ozkaynak<sup>1</sup>, Arastoo Khajehdehi<sup>2</sup>, Ahmet Gullu<sup>2</sup>,  
Faraz Azizisales<sup>2</sup>, Ercan Yuksel<sup>\*3</sup> and Faruk Karadogan<sup>4</sup>

<sup>1</sup> *Beykent University, Department of Civil Engineering, Maslak, Istanbul, Turkey*

<sup>2</sup> *Istanbul Technical University, Institute for Science and Technology, Maslak, Istanbul, Turkey*

<sup>3</sup> *Istanbul Technical University, Faculty of Civil Engineering, 34469, Maslak, Istanbul, Turkey*

<sup>4</sup> *Isik University, Department of Civil Engineering, Sile, Istanbul, Turkey*

(Received July 11, 2016, Revised December 1, 2017, Accepted May 10, 2018)

**Abstract.** Seismic excitations may impart a significant amount of energy into structures. Modern structural design attitudes tend to absorb some part of this energy through special dissipaters instead of heavy plastic deformations on the structural members. Different types of dissipater have been generated and utilized in various types of structures in last few decades. The expected earthquake damage is mainly concentrated on these devices and they may be replaced after earthquakes. In this study, a low-cost device called *energy dissipative steel cushion* (EDSC) made of flat mild steel was developed and tested in the Structural and Earthquake Engineering Laboratory (STEELab) of Istanbul Technical University (ITU). The monotonic and cyclic tests of EDSC were performed in transversal and longitudinal directions discretely. Very large deformation capability and stable hysteretic behavior are some response properties observed from the tests. Load vs. displacement relations, hysteretic energy dissipation properties as well as the closed form equations to predict the behavior parameters are presented in this paper.

**Keywords:** steel cushion; dissipation; energy dissipater; fuse element; hysteretic energy

### 1. Introduction

The overall earthquake behavior of a building is mainly governed by the performance of structural members and connections. In the traditional design philosophy, seismic input energy is substantially dissipated through the inelastic deformations of the structural members. In this philosophy, remarkable residual damage inevitably forms on the members. Recently, energy dissipation using dissipative devices has become increasingly important in the engineering applications. The damage is concentrated mainly on the dissipative devices, which can be replaced easily after disturbing earthquakes. Hence, they reduce the inelastic demands of the primary structural elements.

Although there are different types of dissipative devices in the application, the most commonly used one is metallic dissipaters. They absorb seismic energy through the plastic deformation of metals. There is considerable interest in determining the characteristics of metallic dissipaters both in an experimental and analytical manner in the literature. The metallic dissipaters are able to be classified as per *flexural types* (hourglass shape ADAS (Bergman and Goel 1987), triangular shape TADAS (Tsai *et al.* 1993)), *shear types* (YSPD (Chan *et al.* 2009)) and *axial types* (the buckling restrained brace, Black *et al.* (2004)).

Preliminary tests were performed on flat U-strip type steel dissipaters, whose relative motion is directed parallel to adjacent surfaces, which might be an important energy-absorption source through rolling and bending, Kelly *et al.* (1972). Rai and Wallace (1998) performed a study of aluminum shear links with low-yield strength to increase seismic performance of the frames. The link provided significant energy dissipation. Another experimental study on the determination of behavior of the shear connectors was conducted by Shultz and Magana (1996). They investigated the performance of U-shaped flexure plate (UFP) connectors, which were used as horizontal and vertical joint connectors in precast PRESSSS test buildings. UFP was proposed as an energy-dissipating flexible connector in which the bending action induced by rolling of the U-plate on a straight steel plate resists vertical shear force. In a jointed wall system, the energy-dissipater type steel members were studied in PRESSSS program, Priestley *et al.* (1999). The test building included an un-bonded post-tensioned precast wall system consisting of two walls and several UFP connectors along the vertical joint to resist lateral forces in one direction. It performed very well and no structural damage was observed during the seismic testing. Gang and Hongnan (2013) presented two dampers named the round-hole metallic damper (RHMD) and double X-shaped metallic damper (DXMD). It was shown that the metallic dampers not only provide stiffness but also have the ability to dissipate energy. Chan and Albermani (2008) performed cyclic tests on the steel slit damper (SSD), that was fabricated from standard structural wide-flange section with a number of slits cut on its web. They aimed to investigate the effects of the device's geometrical

\*Corresponding author, Ph.D., Professor,  
E-mail: [yukselerc@itu.edu.tr](mailto:yukselerc@itu.edu.tr)

<sup>a</sup> Professor

<sup>b</sup> Professor

parameters. Experiments showed that the device yielded at a small angular distortion and dissipated considerable amount of energy. Henry *et al.* (2009) proposed a new type O-connector to be utilized on the wall system. The connector was able to dissipate significant amount of energy. However, some out-of-plane deformations were observed during the experiments. It was restricted by installing some additional steel elements. Maleki and Bagheri (2010) studied the behavior of steel pipes, bare and filled with concrete, under cyclic shear to examine the possibility of using them as a seismic damper. The test results showed that the bare steel pipes are capable of absorbing a large amount of energy under a severe cyclic shear load with stable hysteretic behavior. This behavior was also simulated using the finite element method. Gray *et al.* (2010) tested metallic seismic devices used in concentrically braced frames, which were designed to achieve a stable symmetric inelastic response through flexural yielding of the metallic slices. Karalis *et al.* (2011) performed both experimental and numerical work to determine the efficiency of a steel link element having an I-shaped cross-section connected to the RC frame through bracing elements. The energy was dissipated through the steel-link element. It was concluded that the use of steel-link elements can considerably increase the strength, stiffness and energy dissipation capacity of the frame. Sahoo *et al.* (2015) tested metallic devices consisting of series steel plates. End plates with an X-configuration were allowed to yield under flexural action, whereas rectangular web plate was allowed to dissipate energy through shear yielding. Finite element analysis was carried out to predict the ultimate resistance and hysteretic response. Koetaka *et al.* (2005) proposed a new system for the beam-to-column moment connections. The hysteretic dampers were bolted at flanges of the column to the wide-flange beam. The cyclic behavior of the proposed connection was determined through six experiments performed on the full-scale specimens. They resulted that all inelastic deformations were localized in the dampers while the beam and column remained essentially in elastic range.

In this paper, a low-cost steel dissipater so-called *energy dissipative steel cushion* (EDSC) is presented. It was originally conceived to be utilized underneath and between reinforced concrete (RC) claddings of precast construction within the framework of the Safecladding Project (2015). The proposed application details are given in Fig. 1. It is obvious EDSC made of mild steel with low-profile workmanship can be utilized in the other fields of civil engineering. Some other types of connection devices were also studied in the Safecladding Project, Dal Lago *et al.* (2017a, b, c), Negro and Tornaghi (2017), Toniolo and Dal Lago (2017), Zoubek *et al.* (2016a, b).

A flat steel strip is simply bent to achieve the preferred geometry and the ends are properly welded. Those are the essential steps of the production of EDSC. Preliminary investigations on EDSC were accomplished by some researchers in the Safecladding team. Özkaynak *et al.* (2014) performed experimental study to discuss the effects of material quality and the location of welding section on the behavior of EDSC. The experiments resulted that the

specimens made of stainless steel had less strength and energy dissipation capacity compared with mild steel. The position of welding section had important effect on the global behavior of EDSC made of stainless steel. The better performance was obtained from the specimen in which the welding positioned at mid-height of the device. Özkaynak *et al.* (2015) performed experimental studies on the limited number of specimens to identify cyclic behavior of SCs under varying axial stresses. The longitudinal shear behavior for two axial compressive loads was studied. The tests revealed that transversal stress level and its direction are effective variables on strength of EDSC. Güllü *et al.* (2015) and Smyrou *et al.* (2014) performed some studies to generate the numerical models of EDSC through different finite elements. Güllü *et al.* (2016) investigated cyclic behavior of EDSCs under monotonic and cyclic transversal loading. The monotonic test results were simulated by finite element analyses. Yüksel *et al.* (2017) studied the behavior of EDSCs subjected to the simultaneous actions of longitudinal and transversal loading. The experiments resulted that energy dissipation capacity increase with the increment of compressive force acting in the transversal direction. Özkaynak (2017a, b) studied the effects of EDSC on the earthquake behavior of RC structures. It was shown that EDSC is efficient to increase the seismic performance of RC structures.

The objective of this paper is to determine the characteristics of EDSC and to evaluate its effectiveness in energy dissipation. The methodology is based on the intensive experimental works and an attempt to generate the closed form equations for the design purposes. Thickness of steel plate and loading type are the main parameters. The rationale of this work is to generate a metallic low-cost energy dissipative device that could be employed in RC, steel and wood structures.

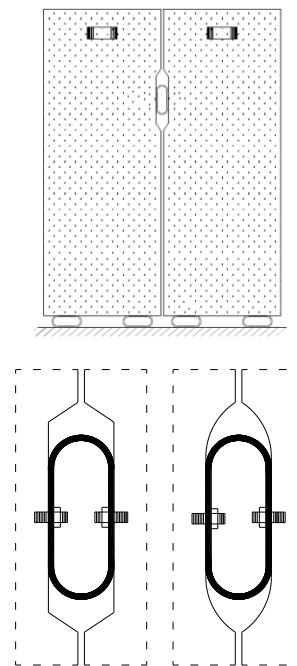


Fig. 1 The application of EDSC in the precast construction

## 2. Specimen, loading and measuring systems

The uni-axial quasi-static tests for two main directions were carried out to determine the monotonic and cyclic behavior of EDSC. It has a specific shape with the capability of rolling and bending actions under shear (longitudinal) loading. Additionally, the plasticized section replaces during the movement.

EDSC is easily manufactured by rolling a strip of flat steel plate. Ends of the plate are connected by proper welding. The cross sectional geometry consists of three parts i.e. two semi-circles at both ends and a rectangle at the middle. The welding section matches to mid-height where the holes are engendered for the connection of the device.

According to results of the numerical studies performed in Safelcladding Project (2015), longitudinal (shear) displacement demand of the connectors (EDSC) between cladding-to-cladding and cladding-to-structure were calculated as 200 mm for the design earthquake. This evidence was utilized in the determination of EDSC geometry, Fig. 1. The cross-sectional dimensions are  $d = 100$  mm and  $h = 250$  mm, and depth is  $b = 100$  mm, Fig. 2. Three alternative plate thicknesses were utilized in this study, namely 3, 5 and 8 mm. The general dimensions (a, b, d) of all specimens are identical.

The tensile test results obtained from the coupon tests are illustrated in Fig. 3. Average tensile strengths determined for 3, 5 and 8 mm thick plates were 410 MPa, 390 MPa and 450 MPa, as well as ultimate strains were

28%, 40% and 40%, respectively.

EDSC has some advantages compared with U-shaped flexural dampers which are also effective in the energy dissipation. Longitudinal displacement capacity of U-shaped dampers is quite low. EDSC is a statically indeterminate member due to its closed geometry. So, the contribution of EDSC to the global strength is greater than U-shaped dampers.

The multi-purpose testing device was designed and produced for the tests, Figs. 4 and 5. The device consists of two fixed and one sliding stiff steel member.

EDSC was positioned between the fixed and the sliding stiff plates for shear testing. Out-of-plane displacements of the sliding plates were restricted by the welded steel plates, Fig. 5. Two vertically and two horizontally oriented displacement transducers were utilized to measure the possible displacements of EDSC. Strain measurements were performed at different sections by means of post-yield strain gauges as illustrated in Fig. 6.

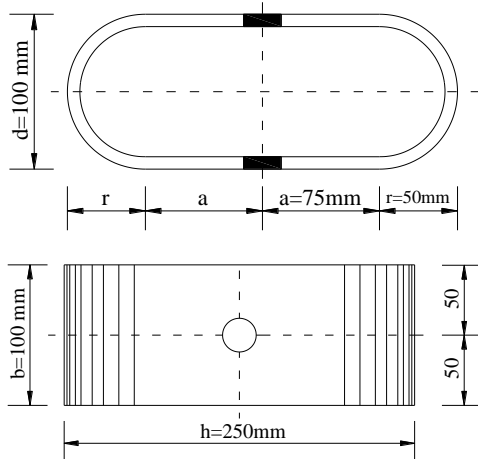


Fig. 2 Geometry of EDSC made of 8 mm thick plate

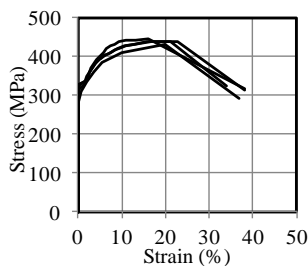


(a) Axial (transversal) loading (Position A)

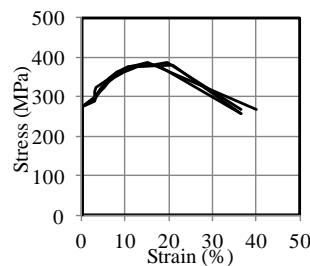


(b) Shear (longitudinal) loading (Position B)

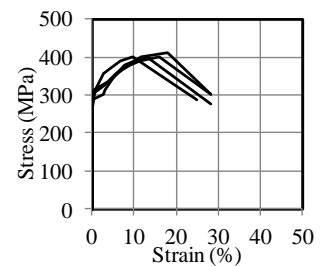
Fig. 4 General views of the homemade testing set-up



(a) 8 mm thick steel cushion



(b) 5 mm thick steel cushion



(c) 3 mm thick steel cushion

Fig. 3 Stress-strain relations obtained from the coupon tensile tests

EDSC was positioned horizontally on the leftmost cantilever for axial loading tests. The actuator's swivel head was kept in a lateral position by the help of cylindrical guiders, Fig. 4(a). Horizontally oriented steel plates transferred compressive force to EDSC while tension force was transferred directly by the connection bolts. This results a non-symmetrical axial behavior. Two vertical displacement transducers were used to measure axial displacement of the specimen. Moreover, two strain gauges were located on external vertexes of the specimens, Fig. 6(b). Strain gauge measurements were used to detect stress concentrations and yielding on EDSC.

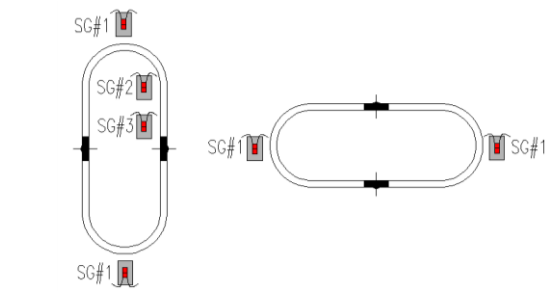
The applied testing program is depicted in Fig. 7. Monotonic and cyclic tests were performed for each type of loading and for all thicknesses. Indeed, thickness of steel plate used for EDSC and type of loading are main variables of the study.

The testing protocol based on the expected ultimate drifts was selected in accordance with the recommendations of FEMA461 (2007). Regarding the expected deformability of the specimen, the target displacements were derived by multiplying the " $a_i/a_{10}$ " ratios specified in FEMA461 with the related dimensions of EDSC. Ten distinct displacement targets were defined and two consecutive identical cycles were applied for each displacement target. The applied displacement protocols are presented in Fig. 8.

### 3. Experimental results

#### 3.1 Axial tests

Force vs. displacement cycles obtained from cyclic and



(a) Cyclic shear tests (b) Cyclic axial test

Fig. 6 Straingauge location of the specimens

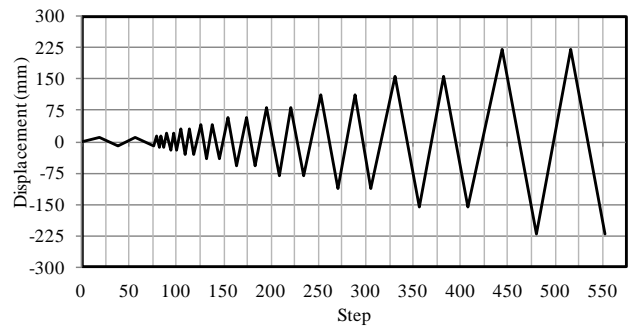
monotonic axial tests as well as the corresponding deformed shapes are presented in Figs. 9, 10 and 11, for distinct plate thicknesses. The monotonic tests yield an envelope that covers the cyclic test results.

The ultimate compressive and tensile strengths achieved are 11 kN and 5 kN respectively. In the evaluation of force vs. displacement relationship given in Fig. 9(a), one can see a minor difference in the results of monotonic and cyclic tests especially at the larger displacements.

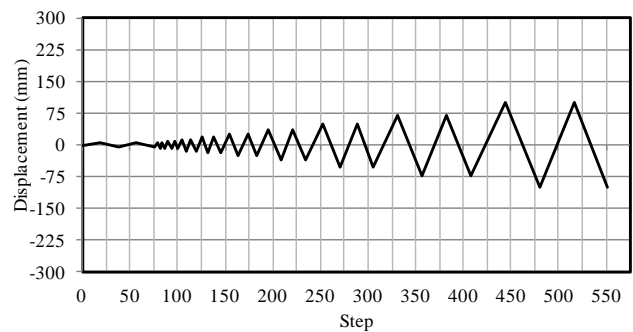
For  $t = 5$  mm, it can be seen that there is a slight divergence in the results of monotonic and cyclic tests, Fig. 10(a). In cyclic loading, ultimate compression strength achieved is 30 kN whereas tensile strength is 10 kN.

For 8 mm-thick plate, ultimate compression strength obtained in the cyclic test is 100 kN while tension strength is 30 kN, as observed in Fig. 11(a).

The load carrying mechanisms are quite different in



(a) Shear test



(b) Axial test

Fig. 8 Drift-based cyclic uni-axial displacement protocols applied to EDSC

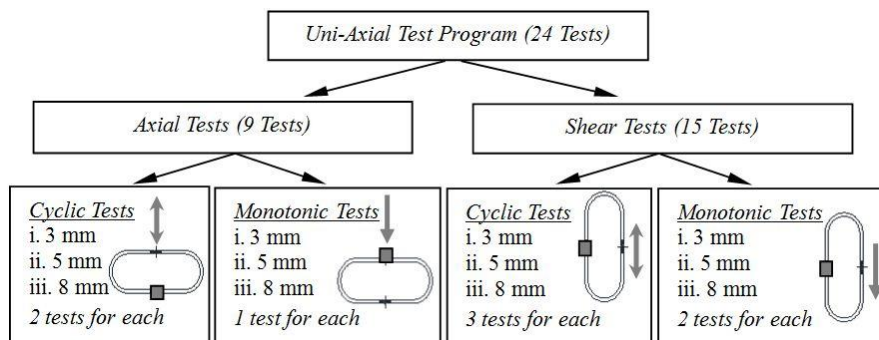


Fig. 7 Summary of the test program



Fig. 9 Cyclic and monotonic axial test results for EDSC with  $t = 3$  mm thickness

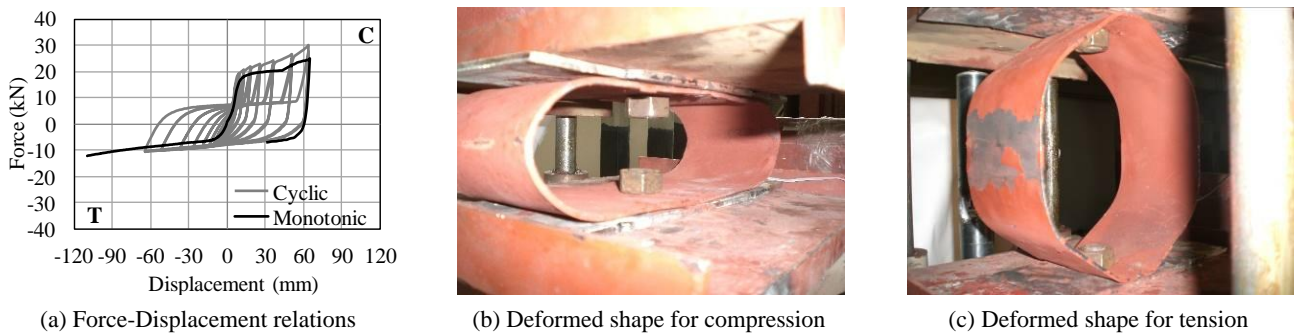


Fig. 10 Cyclic and monotonic axial test results for EDSC with  $t = 5$  mm thickness



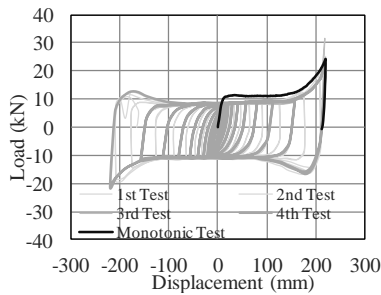
Fig. 11 Cyclic and monotonic axial test results for EDSC with  $t = 8$  mm thickness



Fig. 12 Cyclic and monotonic shear test results for EDSC with  $t = 3$  mm thickness

tension and compression cases. The bolts and their adjacent area are active in tension force. However compressive force is transferred by surfaces of EDSC. So, the specimens had dissimilar tension and compression strengths.

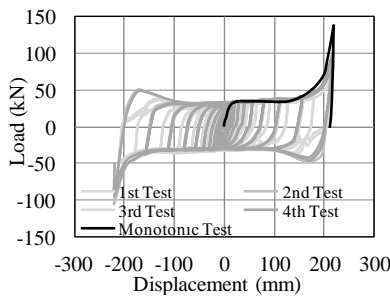
The displacement capacity in compression is restricted by the clear distance between head of the nuts. However, the displacement capacity in tension is directly related to the length of straight part ( $2 \times a$ ) of EDSC, see Fig. 3.



(a) Force-Displacement relations



(b) Deformed shape

Fig. 13 Cyclic and Monotonic Shear Test Results for EDSC with  $t = 5$  mm Thickness

(a) Force-Displacement relations



(b) Deformed shape

Fig. 14 Cyclic and monotonic shear test results for EDSC with  $t = 8$  mm thickness

### 3.2 Shear tests

Force vs. displacement cycles obtained from cyclic and monotonic shear tests and the corresponding deformed shapes for EDSCs made of 3, 5 and 8 mm-thick plates are presented in Figs. 12, 13 and 14, respectively. Generally, monotonic test results cover those of the cyclic tests. Symmetrical behavior is observed for all specimens subjected to cyclic shear effects.

EDSC with 3 mm thickness had a nominal strength of 3.5 kN with a maximum displacement capacity of 220 mm. The yielding was determined at 15 mm according to the strain gauge measurements.

EDSC with thickness of 5 mm had a nominal strength of 10 kN with a maximum displacement capacity of 220 mm. The yielding was determined at 12 mm according to the strain gauge measurements.

EDSC with thickness of 8 mm had a nominal strength of 35 kN and a maximum displacement capacity of 220 mm.

The yielding was determined at 10 mm displacement according to the strain gauge measurements. The sharp increments recorded for stiffness observed at 200 mm displacement level were simply due to the contact of bolts on the steel cushion.

Shear strength of the specimen with 8 mm plate thickness is 7.68 times bigger than shear strength of the specimen with 3 mm plate thickness. One can calculate this strength increment by multiplying ratio of squares of the plate thicknesses ( $82/32 = 7.11$ ) with ratio of material yield strength ( $325 \text{ MPa}/300 \text{ MPa} = 1.08$ ), see Eq. (8).

## 4. Evaluation of experimental results

The test results are evaluated below in terms of various structural parameters for the applied loading type. The parameters taken into consideration are yielding force and displacement, stiffness, strength, ductility, equivalent

Table 1 Summary of test results under compression stress

|                   | Thickness  | Initial stiffness<br>$K_0$ kN/mm | Yield force<br>(kN) | Max force<br>(kN) | Yield disp.<br>$D_y$ (mm) | Ultimate disp.<br>$D_u$ (mm) | Ductility<br>$\mu$ |
|-------------------|------------|----------------------------------|---------------------|-------------------|---------------------------|------------------------------|--------------------|
| Monotonic Loading | $t = 3$ mm | 0.57                             | 6.04                | 10.78             | 10.52                     | 57.53                        | 5.47               |
|                   | $t = 5$ mm | 1.59                             | 16.71               | 23.90             | 10.52                     | 57.01                        | 5.42               |
|                   | $t = 8$ mm | 5.81                             | 60.44               | 110.9             | 10.40                     | 57.21                        | 5.49               |
| Cyclic Loading    | $t = 3$ mm | 0.64                             | 6.11                | 10.21             | 9.52                      | 62.98                        | 6.62               |
|                   | $t = 5$ mm | 1.96                             | 18.65               | 27.34             | 9.53                      | 63.99                        | 6.72               |
|                   | $t = 8$ mm | 8.78                             | 51.02               | 98.37             | 5.81                      | 58.05                        | 9.99               |

Table 2 Summary of test results under tensile stress

|                   | Thickness  | Initial stiffness $K_0$ kN/mm | Yield force (kN) | Max force (kN) | Yield disp. $D_y$ (mm) | Ultimate disp. $D_u$ (mm) | Ductility $\mu$ |
|-------------------|------------|-------------------------------|------------------|----------------|------------------------|---------------------------|-----------------|
| Monotonic Loading | $t = 3$ mm | 0.20                          | 2.70             | 4.46           | 13.79                  | 80.42                     | 5.83            |
|                   | $t = 5$ mm | 0.57                          | 5.95             | 9.75           | 10.49                  | 80.41                     | 7.67            |
|                   | $t = 8$ mm | 2.16                          | 22.9             | 41.18          | 10.60                  | 80.02                     | 7.55            |
| Cyclic Loading    | $t = 3$ mm | 0.29                          | 2.77             | 3.88           | 9.50                   | 61.96                     | 6.52            |
|                   | $t = 5$ mm | 0.79                          | 7.47             | 10.58          | 9.49                   | 61.98                     | 6.53            |
|                   | $t = 8$ mm | 2.60                          | 21.18            | 32.00          | 8.14                   | 56.99                     | 7.00            |

damping and energy dissipation capacities.

#### 4.1 Axial tests

The results obtained from the axial loading tests involving elastic and inelastic properties are summarized in Tables 1 and 2. The first parts of the tables contain monotonic test results while the rest is related to cyclic loading. Although both types of loading give similar results for 3 and 5 mm- thick plates, the results are different for 8 mm in the case of compression, Table 1. On the other hand, both types of loading give similar results for all plate thicknesses in the case of tension loading, Table 2.

##### 4.1.1 Yielding displacement, yielding and ultimate strengths

The increment of plate thickness of EDSC results in lower yielding displacement and larger yielding force, Fig. 15.

Variation of ultimate strengths in terms of the plate thickness of EDSC is illustrated in Fig. 16, for diverse types of loadings. It shows the quadratic relationship between yielding and ultimate strength with the plate thickness of EDSC.

##### 4.1.2 Stiffness and ductility

The cyclic axial behavior of EDSC is determined in terms of normalized stiffness vs. displacement. The normalized stiffness of a cycle is obtained by dividing its secant stiffness with the initial one. The relations between

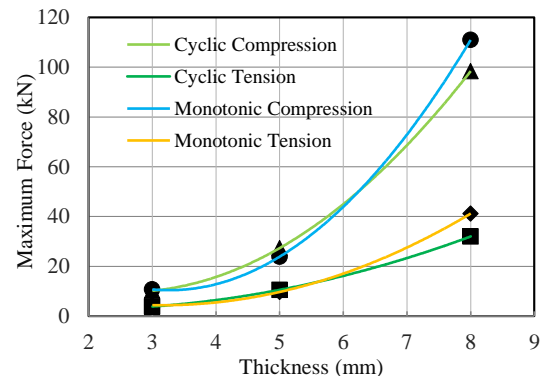


Fig. 16 Ultimate strengths for tension and compression

the normalized stiffness vs. displacement show a decaying form, which is common for all diverse thicknesses, Fig. 17(a). The variation of normalized stiffness is independent of thickness of the plate. The variation of ductility is quantified by dividing the ultimate displacement by the yielding displacement, with respect to plate thickness of EDSC in Fig. 17(b). It shows that the ductility ratio increases with the increment of plate thickness for cyclic and monotonic tension cases.

The ratio of secant stiffness in tension and compression sides of cyclic axial loading for each plate thickness is presented in Fig. 18. The secant stiffness ratio increases with the increment of axial displacement. Hence, non-symmetric behavior arises through the increment of axial displacement.

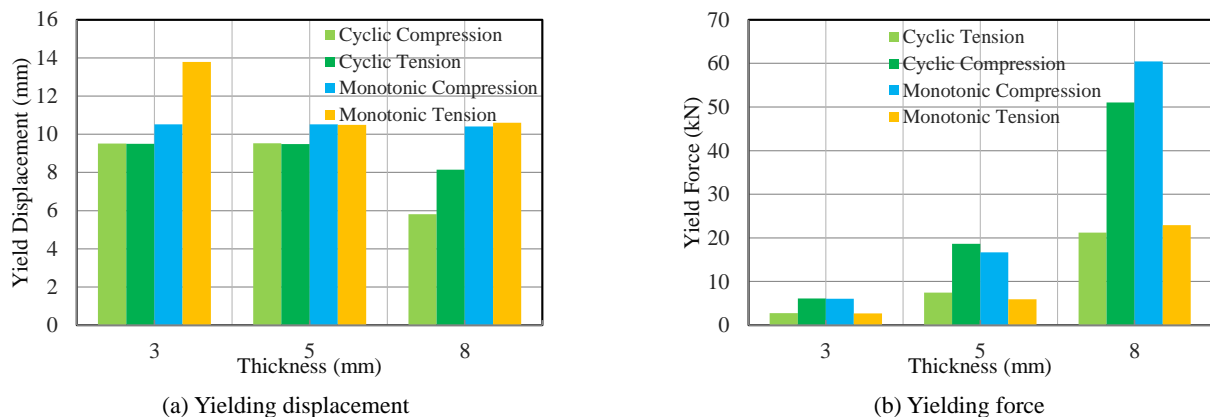


Fig. 15 Yielding force variations in terms of thickness

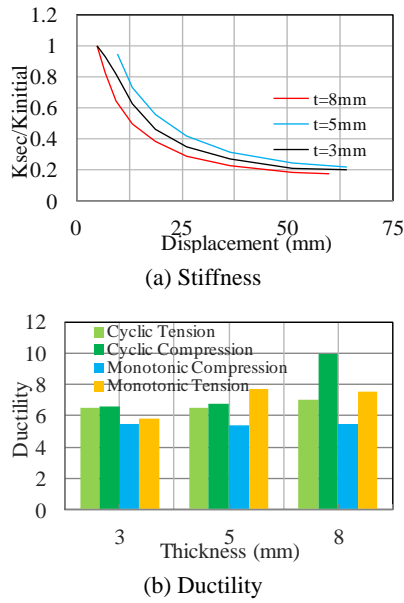


Fig. 17 Displacement vs. normalized stiffness and thickness vs. ductility for axial loading

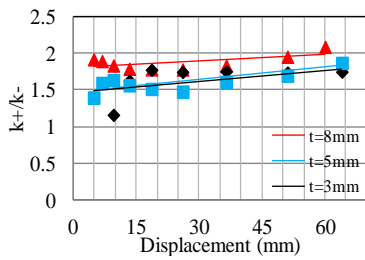


Fig. 18 Secant stiffness ratio variations with respect to the displacement

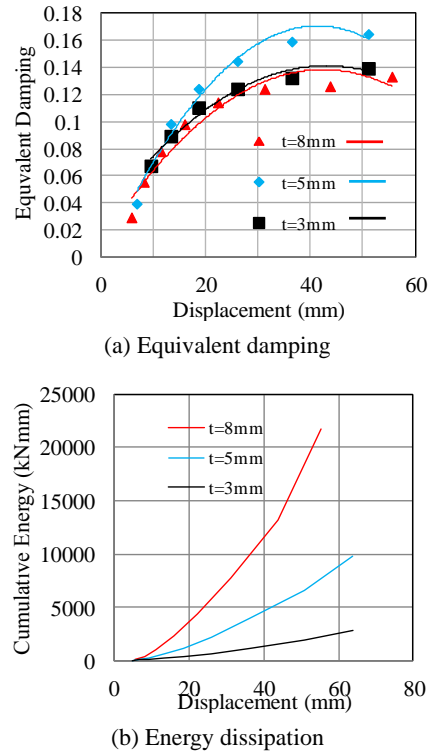


Fig. 19 Equivalent damping and energy dissipation capacity

#### 4.1.3 Equivalent damping ratio and energy dissipation

The equivalent damping ( $\zeta_{eq}$ ) is calculated using Eq. (1), Chopra (1995), in terms of the dissipated energy ( $E_H$ ) and strain energy ( $E_{S0}$ ).

$$\zeta_{eq} = (1/4\pi) (E_H/E_{S0}) \tag{1}$$

Table 3 Summary of experimental results derived from cyclic and monotonic shear tests

| Thickness | Loading | Test # | Initial stiffness $K_0$ (kN/mm) | Yield force (kN) | Max force (kN) | Yield disp. $D_y$ (mm) | Ultimate disp. $D_u$ (mm) | Ductility $\mu$ |
|-----------|---------|--------|---------------------------------|------------------|----------------|------------------------|---------------------------|-----------------|
| t = 3 mm  | Cyclic  | 1      | 0.13                            | 2.94             | 4.25           | 22.03                  | 178.12                    | 8.09            |
|           | Cyclic  | 2      | 0.17                            | 1.82             | 4.12           | 10.59                  | 157.09                    | 14.83           |
|           | Cyclic  | 3      | 0.21                            | 3.03             | 3.81           | 14.97                  | 157.08                    | 10.50           |
|           | Cyclic  | 4      | 0.18                            | 2.70             | 3.48           | 14.95                  | 156.90                    | 10.50           |
|           | Mon.    | 1      | 0.27                            | 3.97             | 5.12           | 14.96                  | 179.13                    | 11.98           |
| t = 5 mm  | Cyclic  | 1      | 0.66                            | 6.93             | 11.73          | 10.55                  | 157.45                    | 14.93           |
|           | Cyclic  | 2      | 0.82                            | 9.82             | 14.25          | 12.01                  | 178.05                    | 14.83           |
|           | Cyclic  | 3      | 0.70                            | 7.36             | 11.38          | 10.55                  | 157.88                    | 14.96           |
|           | Cyclic  | 4      | 0.68                            | 7.23             | 11.80          | 10.56                  | 157.18                    | 14.88           |
|           | Mon.    | 1      | 0.91                            | 10.0             | 14.51          | 10.94                  | 180.13                    | 18.01           |
| t = 8 mm  | Cyclic  | 1      | 2.01                            | 24.17            | 45.62          | 12.0                   | 178.71                    | 14.90           |
|           | Cyclic  | 2      | 2.71                            | 28.63            | 40.24          | 10.56                  | 157.15                    | 14.89           |
|           | Cyclic  | 3      | 2.84                            | 29.95            | 38.45          | 10.56                  | 157.08                    | 14.88           |
|           | Cyclic  | 4      | 2.71                            | 28.52            | 38.24          | 10.53                  | 156.82                    | 14.89           |
|           | Mon.    | 1      | 2.39                            | 25.3             | 52.92          | 10.58                  | 180.61                    | 17.07           |

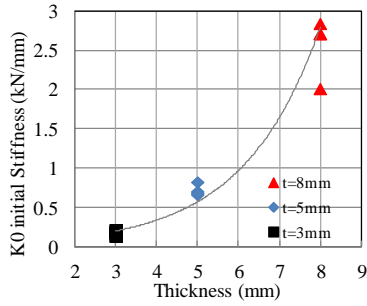
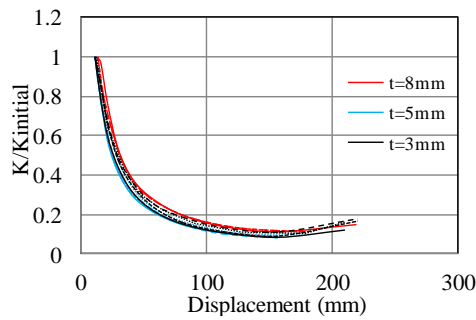
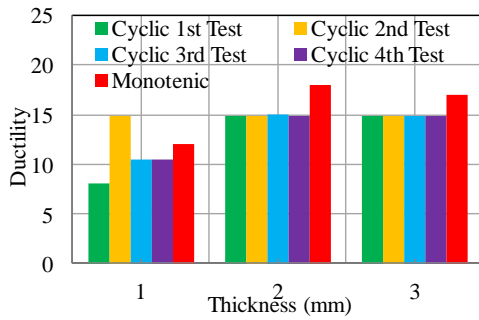


Fig. 20 Initial stiffness and yielding displacement variations in terms of thickness



(a) Normalized stiffness



(b) Ductility

Fig. 21 Displacement vs. normalized stiffness and thickness vs. ductility for axial loading

The maximum  $\zeta_{eq}$  of the tested specimens varies between 13-18%, Fig. 19(a). It gradually increases by the increment of axial displacement. A 5 mm thick specimen yields more equivalent damping than 3 and 8 mm thick specimens. The possible reason for the disordering is that the yielding strength of the 5 mm thick plate is lower than the others, Fig. 2. The axial displacement vs. cumulative hysteretic energy diagrams that are deliberated as the enclosed area of the force vs. displacement curves are presented in Fig. 19(b). The energy graphs clearly show that the energy dissipation capacity is proportional to the plate thickness of EDSC.

#### 4.2 Shear tests

The experimental results derived from cyclic and monotonic shear tests for the three distinct plate thicknesses of EDSC are summarized in Table 3. They show relatively high scattering for the yielding properties in the cyclic tests

of 3 mm-thick EDSC plates.

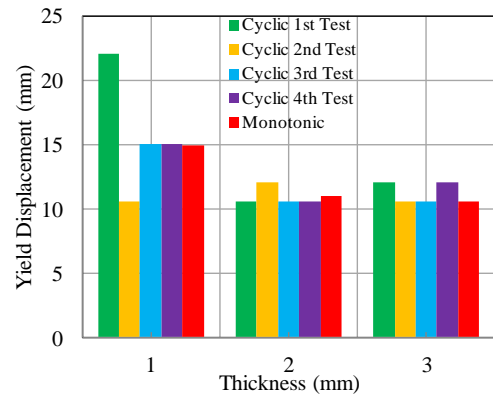
##### 4.2.1 Stiffness and ductility

The initial stiffness,  $K_0$ , of the specimens is illustrated in Fig. 20. It clearly shows that a quadratic relation exists between stiffness and plate thickness of EDSC.

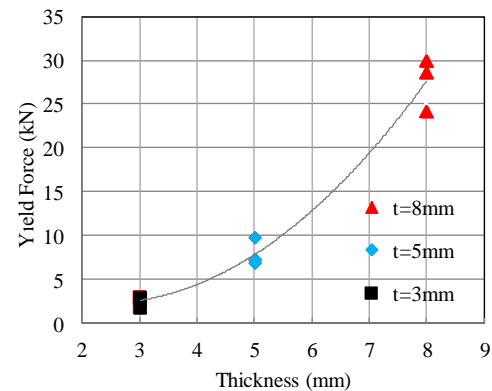
The cyclic shear behavior of EDSC is determined in terms of normalized stiffness vs. displacement. The normalized stiffness vs. displacement relation deteriorates smoothly for all achieved tests, Fig. 21(a). The variation of ductility with respect to the plate thickness of EDSC is presented in Fig. 21(b). It shows that the ductility ratio increases with the increments in plate thickness of EDSC. However, the results corresponding to 5 mm-thick plates are not consistent with the tendency because of the aforementioned material yielding properties.

##### 4.2.2 Yielding displacement, yielding and ultimate strengths

Yielding displacement and yielding force variation in respect to the plate thickness are presented in Fig. 22(a) and 22(b), respectively. The yield displacement varies conversely with the increment of plate thickness of EDSC. In the case of 3 mm thickness, some scattering between the test results is observed. Although similar results were obtained for 5 and 8 mm-thick specimens, it is predicted that the aforementioned yielding property is the potential reason of the pertinent disorder. The increments in plate



(a) Yielding displacement



(b) Yielding force

Fig. 22 Yielding displacement variations in terms of thickness

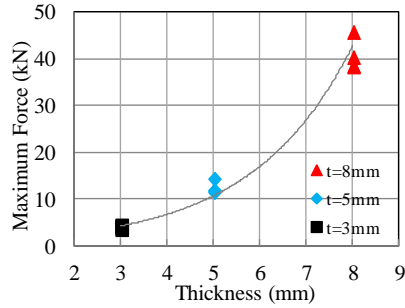
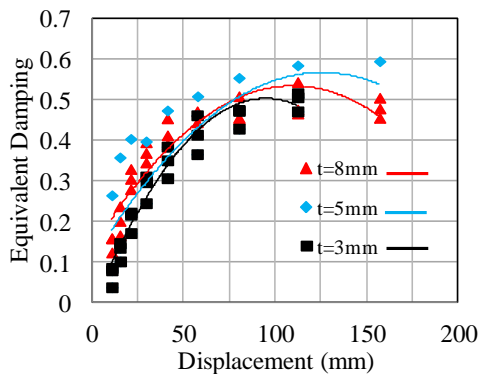


Fig. 23 Maximum force variations in terms of thickness

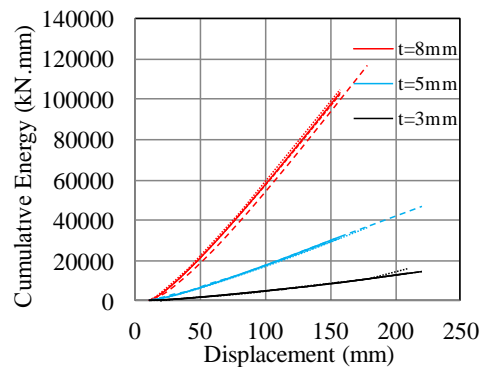
thickness of EDSC results in larger yielding and maximum forces. Even if there are some deviations in the results of the repetitive specimens, the quadratic relation between plate thicknesses can be assessed and the observed yielding and maximum forces are as expected, Fig. 23.

4.2.3 Energy dissipation and equivalent damping

The maximum equivalent damping ratios of the tested specimens range from 55% to 60% Fig. 24(a). They progressively increase with the increment of displacement. In a similar manner, 5 mm-thick specimen produces a higher damping ratio than the others. The shear displacement vs. cumulative hysteretic energy diagrams obtained for the selected specimens are presented in Fig. 24(b). It should be noted that the energy dissipation capacity is quadratically related to the plate thickness of EDSC.



(a) Equivalent damping



(b) Cumulative energy dissipation

Fig. 24 Cumulative energy dissipation capacity for cyclic shear tests

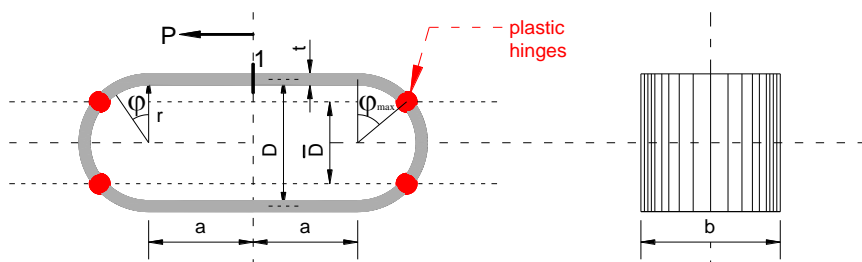


Fig. 25 Geometrical properties of EDSC

5. Closed form equations

Closed form equations to attain elastic and post-yield behavior of EDSC in the case of shear loading are extracted through the classical flexibility method, Gullu *et al.* (2016). These equations are beneficial to design of EDSC for a specific purpose.

The five critical parameters to define the geometry of EDSC are as follows; radius of half circles (*r*), half of the straight part (*a*), width of cushion (*b*), thickness (*t*) and angle between the top point of half circle and any point on circle ( $\varphi$ ) Fig. 25.

EDSC has three redundancies in the flexibility method. The selected redundancies are presented in Fig. 26(a). Due to the symmetrical geometry of EDSC, moment diagrams generated for the selected redundant forces and the external load given in Fig. 26(b) will be symmetric or anti-symmetric. Consequently, the symmetrical redundant forces ( $X_2$  and  $X_3$ ) will be zero for the shear loading. The required moment diagrams for the solution are depicted in Figs. 26(b) and (c). The displacement of EDSC is determined through virtual work theory. Moment diagram for the unit force is given in Fig. 26(d).

The compatibility equation and its terms are defined in Eq. (2). The redundant force of  $X_1$  is determined from Eq. (3). The moment function and position of moment extremum are given by Eqs. (4) and (5), respectively.

$$\delta_{11} = \int \frac{M_1 M_1}{EI} ds \quad \delta_{10} = \int \frac{M_1 M_0}{EI} ds \quad (2)$$

$$\delta_{11} X_1 + \delta_{10} = 0$$

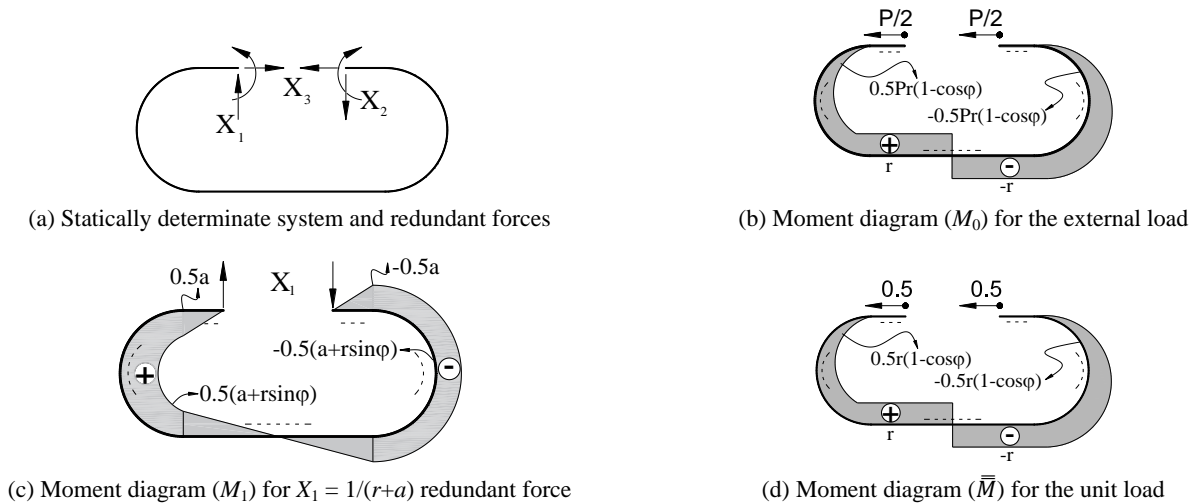


Fig. 26 The application of flexibility method to EDSC

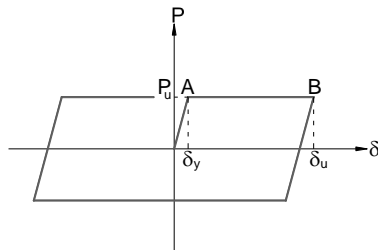


Fig. 27 The elastic-perfectly-plastic backbone curve

$$X_1 = -\frac{\delta_{10}}{\delta_{11}} = -\frac{Pr(a+r)(a^2 + \pi ar + 2r^2)}{4a^3/3 + 2\pi a^2 r + 8ar^2 + \pi r^3} \quad (3)$$

$$M(\varphi) = \frac{Pr}{2}(1 - \cos \varphi) + \frac{a+r \sin \varphi}{a+r} \left[ -\frac{Pr(a+r)(a^2 + \pi ar + 2r^2)}{4a^3/3 + 2\pi a^2 r + 8ar^2 + \pi r^3} \right] \quad (4)$$

$$\varphi_{\max} = \frac{dM(\varphi)}{d\varphi} = 0 \rightarrow \varphi_{\max} = -\frac{1}{2} \log \left( \frac{1.5i\pi r^3 + 12iar^2 - 3a^2r + 2ia^3 - 6r^3 - 3\pi ar^2 + 3i\pi a^2 r}{1.5i\pi r^3 + 12iar^2 + 3a^2r + 2ia^3 + 6r^3 + 3\pi ar^2 + 3i\pi a^2 r} \right) \quad (5)$$

The lateral displacement of EDSC is calculated by Eq. (6) where  $M$  and  $\bar{M}$  represent moment diagrams due to the external loading and the unit force, respectively.

$$\delta_h = \int \frac{M\bar{M}}{EI} ds = \frac{Pr^2}{EI} \left( \frac{5a^4 + 9\pi a^3 r + (36 + 1.5\pi^2)a^2 r^2 + 12\pi ar^3 + (2.25\pi^2 - 12)r^4}{4a^3 + 6\pi a^2 r + 24ar^2 + 3\pi r^3} \right) \quad (6)$$

Four plastic hinges are occurred simultaneously, Fig. 25. Hence yielding force capacity of EDSC is determined by Eq. (8). If  $P_u$  is substituted with  $P$  in Eq. (6), one can reach yielding displacement of  $\delta_y$ .

$$\bar{D} = 2r \cos \phi \quad (7)$$

$$P_u = \frac{f_{yd} b t^2}{\bar{D}} = \frac{f_{yd} b t^2}{2r \cos \phi} \quad (8)$$

The ultimate displacement capacity of EDSC ( $\delta_u$ ) is determined as  $(2 \times a)$ , see Fig. 25.

The *elastic perfectly plastic backbone curve* is proposed here to represent cyclic shear behavior of EDSC, Fig. 27. Critical points of the backbone curve are described as “A” that represents yielding and “B” that represents ultimate point.

The plasticized cross sections are relocated during the rolling action of EDSC.

Comparison of the results derived from the closed form equations with the experimental ones are given in Table 4. It should be noted that maximum relative difference is about 6%.

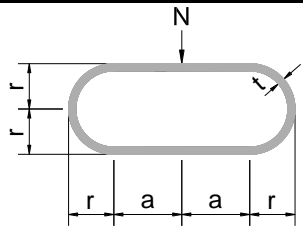
A similar procedure is applied to derive the closed form

Table 4 Comparison of the results for shear

| $t$ (mm) | $\varphi$ (rad) | $P_u$ (kN) |       |             | $\delta_y$ (mm) |       |             |
|----------|-----------------|------------|-------|-------------|-----------------|-------|-------------|
|          |                 | CFE        | Exp.  | R. Dif. (%) | CFE             | Exp.  | R. Dif. (%) |
| 8        | 0.4683          | 26.51      | 29.13 | 4.71        | 9.50            | 10.56 | 5.28        |
| 5        | 0.4759          | 8.14       | 8.48  | 2.05        | 11.72           | 11.94 | 0.93        |
| 3        | 0.4807          | 3.13       | 3.03  | 1.62        | 21.99           | 19.50 | 6.00        |

\*CFE: The closed form equations, Exp.: Experimental study, R. Dif.: Relative difference

Table 5 Closed form equations for axial loading



$N > 0$  Compressive Force  
 $N < 0$  Tensile Force

Moment  $M(\phi) = \frac{N}{2} \left( \frac{2r^2 - a^2}{\pi r + 2a} - r \sin \phi \right)$   $M_{\max} = M(\phi_{\max})$

Location of moment extremum  $\phi_{\max} = \frac{\pi}{2}$

Vertical displacement (Compression)  $\delta_v = \frac{Nr}{2EI} \left( \frac{\pi a^3 + 8a^2 r + 2\pi a r^2 + (\pi^2 - 8)r^3}{2(2a + \pi r)} \right)$

Vertical displacement (Tension)  $\delta_v = \frac{Nr}{EI} \left( \frac{\pi a^3 + 8a^2 r + 2\pi a r^2 + (\pi^2 - 8)r^3}{2(2a + \pi r)} \right)$

$N_u$  (Compression)  $N_{u,comp} = f_{yd} \frac{bt^2}{4}$

$N_u$  (Tension)  $N_{u,ten} = f_{yd} \frac{bt^2}{4} \times \frac{D_{bolthead}}{2a}$

Table 6 Comparison of the results for compressive loading

| $t$<br>(mm) | $N_u$ (kN) |       |             | $\delta_y$ (mm) |       |             |
|-------------|------------|-------|-------------|-----------------|-------|-------------|
|             | CFE        | Exp.  | R. Dif. (%) | CFE             | Exp.  | R. Dif. (%) |
| 8           | 54.40      | 51.44 | 2.80        | 5.18            | 5.60  | 3.90        |
| 5           | 16.87      | 15.91 | 2.93        | 7.59            | 9.71  | 12.25       |
| 3           | 6.75       | 7.30  | 3.92        | 14.52           | 14.13 | 1.37        |

\*CFE: The closed form equations, Exp.: Experimental study,  
R. Dif.: Relative difference

Table 7 Comparison of the results for tensile loading

| $t$<br>(mm) | $N_u$ (kN) |       |             | $\delta_y$ (mm) |       |             |
|-------------|------------|-------|-------------|-----------------|-------|-------------|
|             | CFE        | Exp.  | R. Dif. (%) | CFE             | Exp.  | R. Dif. (%) |
| 8           | 20.74      | 22.65 | 4.40        | 10.36           | 10.21 | 0.73        |
| 5           | 6.44       | 6.09  | 2.79        | 15.19           | 11.09 | 15.60       |
| 3           | 2.57       | 3.12  | 9.67        | 26.68           | 20.1  | 14.07       |

\*CFE: The closed form equations, Exp.: Experimental study,  
R. Dif.: Relative difference

equations for the axial load effect in the elastic range, (Güllü *et al.* 2016). Due to the loading symmetry, the redundant force of  $X_1$  will be zero, Fig. 26(a). The functions of moment, location of moment extremum, vertical displacements and axial load capacities are listed in Table 5. Ultimate compressive displacement is limited with the clear distance between the bolt heads.

The comparisons are accomplished here for the axial loading. The results are discussed in Tables 6 and 7. The maximum relative difference is about 16%.

## 6. Conclusions

A low-cost EDSC made of mild steel was developed for use in various engineering applications. A comprehensive test campaign was accomplished to extract the behavior of EDSC under the uni-axial loadings. Great deformation capability and stable hysteretic loops are the most important features of EDSCs. The following conclusions could be made:

- EDSCs demonstrate stable and large force-displacement hysteretic behavior, which might be a substantial source of energy dissipation for the applied uni-axial loadings.
- It is observed that the most-effective parameter on the behavior of EDSC is plate thickness. The stiffness, strength, ductility and energy dissipation capacity are all thickness-dependent properties. There are quadratic relations between EDSC plate thickness and those response parameters. Though stiffness degradation vs. displacement relationship is independent from the plate thickness.
- EDSC has a great displacement capacity. The ultimate displacement capacity will be as large as the length of the straight part of EDSC.
- Non-symmetric force-displacement relationships

are obtained in the axial loading.

- The equivalent damping ratio determined in the shear loading is about 55%. Though it is in the range of 13-18% in the axial loading.
- The closed form equations are recommended to estimate *uni-axial elastoplastic shear behavior* of EDSC. When the equation based results are compared with those of the tests, the obtained maximum relative difference is about 6%.
- The closed form equations suggested for *elastic axial behavior* of EDSC result maximum relative difference of 16%.

## Acknowledgments

The research presented herein was conducted in the framework of the FP7 project “SAFECLADDING: Improved Fastening Systems of Cladding Wall Panels of Precast Buildings in Seismic Zones” research for SME associations, grant agreement number 314122, which was coordinated by Mr. Alessio Rimoldi from BIBM. The financial support provided by the Commission of the European Communities through this project is greatly appreciated. The study was conducted at the Structural and Earthquake Engineering Laboratory (STEELab) of Istanbul Technical University. The support of the laboratory staff and graduate students is gratefully acknowledged.

## References

- Bergman, D.M. and Goel, S.C. (1987), “Evaluation of cyclic testing of steel plate devices for added damping and stiffness”, *UMCE87-10*, Ann Arbor, University of Michigan, IL, USA.
- Black, C.J., Makris, N. and Aiken, I.D. (2004), “Component testing, seismic evaluation and characterization of buckling-restrained braces”, *ASCE J. Struct. Eng.*, **130**(6), 880-894.
- Chan, R.W. and Albermani, F. (2008), “Experimental study of steel slit damper for passive energy dissipation”, *Eng. Struct.*, **30**(4), 1058-1066.
- Chan, R.W., Albermani, F. and William, M.S. (2009), “Evaluation of yielding shear panel device for passive energy dissipation”, *J. Constr. Steel Res.*, **65**(2), 260-268.
- Chopra, A.K. (1995), *Dynamics of Structures: Theory and Applications to Earthquake Engineering*, Prentice Hall, Englewood Cliffs, NJ, USA.
- Dal Lago, B., Biondini, F. and Toniolo, G. (2017a), “Experimental investigation on steel W-shaped folded plate dissipative connectors for horizontal precast concrete cladding panels”, *J. Earthq. Eng.*, **22**(5), 778-800.  
DOI: 10.1080/13632469.2016.1264333
- Dal Lago, B., Biondini, F. and Toniolo, G. (2017b), “Friction-based dissipative devices for precast concrete panels”, *Eng. Struct.*, **147**, 356-371.
- Dal Lago, B., Biondini, F., Toniolo, G. and Tornaghi, M.L. (2017c), “Experimental investigation on the influence of silicone sealant on the seismic behaviour of precast façades”, *Bull. Earthq. Eng.*, **15**(4), 1771-1787.
- FEMA-461 (2007), Interim testing protocols for determining the seismic performance characteristics of structural and nonstructural components; Federal Emergency Management Agency, Washington, DC, USA.
- Gang, L. and Hongnan, N.L. (2013), “Experimental study and application in steel structure of dual functions metallic damper”, *ASCE J. Struct. Eng.*, **9**(3), 247-258.
- Gray, M.G., Christopoulos, C. and Packer, J.A. (2010), “Cast steel yielding fuse for concentrically braced frames”, *Proceedings of the 9th U.S. National and 10th Canadian Conference on Earthquake Engineering*, Toronto, Canada, July.
- Güllü, A., Özkaynak, H., Khajehdehi, A., Gökçe, T., Azizisales, F., Bal, İ.E., Smyrou, E., Yüksel, E. and Karadoğan, F. (2015), “Derivation of the closed form equations for the energy dissipative steel cushions”, *Proceedings of the 14th World Conference on Seismic Isolation, Energy Dissipation and Active Vibration Control of Structures (14WCSI)*, San Diego, CA, USA, September.
- Güllü, A., Yüksel, E., Khajehdehi, A., Karadoğan, H.F. and Özkaynak, H. (2016), “Experimental and analytical evaluation of the axial behaviour of energy dissipative steel cushions”, *Proceedings of 2016 NZSEE Conference*, Christchurch, New Zealand, April. [Poster]
- Henry, R.S., Aaleti, S., Sritharan, S. and Ingham, J.M. (2009), “Concept and finite-element modeling of new steel shear connectors for self-centering wall systems”, *J. Eng. Mech.*, **136**(2), 220-229.
- Karalis, A.A., Georgiadi-Stefanidi, K.A., Salonikios, T.N., Stylianidis, K.C. and Mistakidis, E.S. (2011), “Experimental and numerical study of the behavior of high dissipation metallic device for the strengthening of existing structures”, *Proceedings of COMPDYN 2011 III ECCOMAS Thematic Conference on Computational Methods in Structural Dynamics and Earthquake Engineering*, Corfu, Greece, May.
- Kelly, J.M., Skinner, R.I. and Heine, A.J. (1972), “Mechanisms of energy absorption in special devices for use in earthquake-resistant structures”, *Bull. New Zealand Nat. Soc. Earthq. Eng.*, **5**(3), 63-88.
- Koetaka, Y., Chusilpb, P., Zhangc, Z., Andoa, M., Suitad, K., Inouea, K. and Unoe, N. (2005), “Mechanical property of beam-to-column moment connection with hysteretic dampers for column weak axis”, *Eng. Struct.*, **27**, 109-117.
- Maleki, S. and Bagheri, S. (2010), “Pipe damper, Part I: Experimental and analytical study”, *J. Constr. Steel Res.*, **66**, 1088-1095.
- Negro, P. and Tornaghi, M.L. (2017), “Seismic response of precast structures with vertical cladding panels: the SAFECLADDING experimental campaign”, *Eng. Struct.*, **132**, 205-228.
- Özkaynak, H. (2017a), “Model proposal for steel cushions for use in Reinforced Concrete frames”, *KSCE J. Civil Eng.*, **21**(7), 2717-2727. DOI: 10.1007/s12205-017-0477-1
- Özkaynak, H. (2017b), “The effects of special metallic dampers on the seismic behavior of a vulnerable RC frame”, *Struct. Eng. Mech., Int. J.*, **61**(4), 483-496.
- Özkaynak, H., Gullu, A., Gokse, T., Khajehdei, A., Mahdavi, M., Azizisales, F., Smyrou, E., Bal, İ.E., Yüksel, E. and Karadogan, F. (2014), “Energy Dissipater Steel Cushions”, *Proceedings of the 2nd European Conference on Earthquake Engineering and Seismology*, Istanbul, Turkey, August.
- Özkaynak, H., Güllü, A., Khajehdehi, A., Gökçe, T., Azizisales, F., Bal, İ.E., Smyrou, E., Yüksel, E. and Karadoğan, F. (2015), “Bi-directional loading tests of steel cushions”, *Proceedings of the 14th World Conference on Seismic Isolation, Energy Dissipation and Active Vibration Control of Structures (14WCSI)*, San Diego, CA, USA, September.
- Priestley, M.J., Sritharan, S., Conley, J.R. and Pampanin, S. (1999), “Preliminary results and conclusions from the PRESSS five-story precast concrete test building”, *J. PCI*, **44**(6), 42-67.
- Rai, D.C. and Wallace, B.J. (1998), “Aluminum shear link for enhanced seismic resistance”, *Earthq. Eng. Struct. Dyn.*, **27**(4), 315-342.
- Safecladding (2015), Improved Fastening Systems of Cladding

- Panels for Precast Buildings in Seismic Zones; Research for SME Associations Project FP7-314122.
- Sahoo, D.R., Singhal, T., Taraithia, S.S. and Saini, A. (2015), "Cyclic behavior of shear-and-flexural yielding metallic dampers", *J. Constr. Steel Res.*, **114**, 247-257.
- Shultz, A.E. and Magana, R.A. (1996), "Seismic behavior of connections in precast concrete walls", *Proceedings of Mete A. Sozen Symposium. ACI SP-162*, American Concrete Institute, Farmington Hills, MI, USA.
- Smyrou, E., Gullu, A., Yuksel, E., Ozkaynak, H. and Karadogan, F. (2014), "Modelling of an Energy Dissipator for Precast RC Systems", *Proceedings of the 2<sup>nd</sup> European Conference on Earthquake Engineering and Seismology*, Istanbul, Turkey, August.
- Tsai, K., Chen, H., Hong, C. and Su, Y. (1993), "Design of steel triangular plate energy absorbers for seismic-resistant construction", *Earthq. Spectra*, **9**(3), 505-528.
- Toniolo, G. and Dal Lago, B. (2017), "Conceptual design and full-scale experimentation of cladding panel connection systems of precast buildings", *Earthq. Eng. Struct. Dyn.*, **46**(14), 2565-2586.
- Yuksel, E., Karadogan, F., Ozkaynak, H., Khajehdehi, A., Gullu, A., Smyrou, E. and Bal, I.E. (2018), "Behaviour of steel cushions subjected to combined Actions", *Bull. Earthq. Eng.*, **16**, 707-729.
- Zoubek, B., Fischinger, M. and Isakovic, T. (2016a), "Cyclic response of hammer-head strap cladding-to-structure connections used in RC precast buildings", *Eng. Struct.*, **119**, 135-148.
- Zoubek, B., Fischinger, M. and Isakovic, T. (2016b), "Seismic response of short restrainers used to protect cladding panels in RC precast buildings", *J. Vib. Control*, 1077546316659780.  
DOI: 10.1177/1077546316659780